Nonequilibrium Laminar Boundary-Layer Flow of Ionized Air

F. G. BLOTTNER*
General Electric Company, King of Prussia, Pa.

Numerical calculations of the nonequilibrium ionized air boundary layer on a cone-shaped re-entry vehicle at several flight conditions are determined with a finite-difference scheme. The results of this investigation show that the electron density 15-ft downstream on a cone at re-entry velocity is approximately 10^7 electrons/cm^3 at 150,000-ft alt, whereas at 100,000 ft, the value has increased to 10^{10} electrons/cm^3. This investigation also shows the importance of considering the nonequilibrium aspects of the flow rather than the limiting cases of frozen or equilibrium flow. The study of the chemical reactions shows that atomic oxygen is mainly produced from the dissociation of molecular oxygen, whereas atomic nitrogen results mainly from two of the shuffle reactions. The production of nitric oxide comes from the shuffle reactions. For distances up to 15-ft downstream from the tip and for conditions considered, none of the chemical reactions are near equilibrium.

Nomenclature

A_n, B_n, C_n, D_n = coefficient matrices in the difference equation (12)
c_i = mass fraction of species i, ρ_i/ρ
c_{pi} = specific heat at constant pressure of species i, ft^2/(sec^2-°R)
$\bar{c}_p$ = frozen specific heat at constant pressure of the mixture, $\Sigma_i c_i c_{pi}$, ft^2/(sec^2-°R)
D_{ij} = multicomponent diffusion coefficient, ft^2/sec
$\mathfrak{D}_{ij}$ = binary diffusion coefficient, ft^2/sec
f' = velocity ratio, u/u_e
h = enthalpy, $\Sigma_i h_i c_i$, ft^2/sec^2
h_i = enthalpy of species i, ft^2/sec^2
j_i = mass flux relative to the mass-average velocity, slug/(ft^2-sec)
k = thermal conductivity of mixture, lb/(sec-°R)
k_{fr}, k_{br} = forward and backward rate constants, see Eq. (10)
l = density-viscosity product, $\rho\mu/(\rho\mu)_r$
L_{ij} = multicomponent Lewis-Semenov number, $\bar{c}_p\rho D_{ij}/k$
$\mathfrak{L}_{ij}$ = binary Lewis-Semenov number, $\bar{c}_p\rho\mathfrak{D}_{ij}/k$
L_i^T = thermal Lewis-Semenov number, $\bar{c}_p D_i^T/k$
$\bar{M}$ = molecular weight of the mixture, $1/(\Sigma_i\, c_i/M_i)$, lb/lb-mole
M_i = molecular weight of species i, lb/lb-mole
NI = number of chemical species
NJ = number of chemical species and catalytic bodies
NR = number of chemical reactions
Pr = Prandtl number, $\bar{c}_p\mu/k$
p = pressure, psf
R = universal gas constant, lb-ft^2/(lb-mole-sec^2-°R)
r = distance from axis in axisymmetric problems, ft
T = temperature, °R
u, v = velocity components tangential and normal to body surface, fps
V = transformed normal velocity, Eq. (6a)
w_i = mass rate of formation of species i, lb-sec^2/(ft^4-sec)
w_n = vector for dependent variables
x = distance along surface from leading edge or stagnation point, ft
y = distance along normal from surface, ft
α_{ri}, β_{ri} = forward and backward stoichiometric coefficients
β = pressure gradient parameter, $(2\xi/u_e)(du_e/d\xi)$
γ_i = mass concentration of species i, lb-mole/lb
η = transformed y coordinate
ξ = transformed x coordinate, lb^2-sec^2/ft$^{2(2-j)}$
$\Delta\eta, \Delta\xi$ = step sizes in transformed coordinates
θ = temperature ratio, T/T_e
μ = viscosity, lb-sec/ft^2
ρ = density, lb-sec^2/ft^4
ρ_i = density of species i, lb-sec^2/ft^4

Subscripts

b = conditions at body surface
e = conditions at outer edge of boundary layer
m = designation of mesh point in ξ direction, $\xi = (m-1)\Delta\xi$
n = designation of mesh point in η direction, $\eta = (n-1)\Delta\eta$
r = quantities evaluated at some reference condition
∞ = freestream conditions

Presented as Preprint 64-41 at the AIAA Aerospace Sciences Meeting, New York, January 20–22, 1964; revision received August 6, 1964. Based upon work sponsored by the Ballistic Missiles Division of the U. S. Air Force under Contract AF 04(694)-486. The author wishes to acknowledge the efforts of E. Meyer, who did the programing of the finite-difference scheme and obtained the numerical solutions.

* Specialist, Gasdynamics, Space Sciences Laboratory. Member AIAA.

I. Introduction

FOR high-speed vehicles, the presence of ionized species in the boundary layer contributes to the interference to transmission of electromagnetic signals to and from the vehicle. This problem is particularly important for slender configurations, as the boundary layer is the principal source of high-temperature gas. In addition, a detailed knowledge of the boundary layer at the rear of the vehicle is a necessary initial condition for the study of wake properties that have important bearing on problems of detection and discrimination of re-entry vehicles.

Several methods appeared recently to predict the electron density in the nonequilibrium air boundary layer. The more accurate methods employed have been by Blottner and Lenard,[1] with a finite-difference scheme, and by Pallone, Moore, and Erdos[2] with a multistrip integral technique. The method of "local similarity" has also been applied by Blottner and Lenard,[1] and Lenard[3] to obtain reasonably accurate results; however, the solution of the two-point boundary-value problem requires excessive computation time and is very difficult to obtain downstream. Levinsky and Fernandez[4] have also used "local similarity" with additional simplifying assumptions to obtain approximate solutions for sharp cone boundary-layer flow. This paper is of interest because it has given some indication of how the electron density can be correlated. Another approximate procedure has been proposed by DeRienzo, Wood, Berner, and Teare[5]

which employs a streamtube method that greatly overpredicts the electron density due to the neglect of diffusion.

The present paper gives the details of an implicit finite-difference scheme for solving the partial differential equations for the chemically reacting boundary layer for a multicomponent gas. The present procedure is an extension of the scheme previously employed for a binary gas by Blottner.[6] For the numerical examples, the multicomponent gas is specialized to ionized air with seven species (O_2, N_2, O, N, NO, NO^+, e^-) and 11 chemical reactions. For the ionized species, ambipolar type of diffusion is employed. The thermodynamic and transport properties are determined from kinetic theory with the currently available information employed. With this gas model and the numerical method, the boundary-layer flow on a cone at several altitudes and reentry velocities has been determined. The various species in the flow and the electron density are presented in addition to the temperature in the boundary layer. The significance of the various reactions in producing the species is discussed.

II. Method of Analysis

A. System of Equations

The boundary-layer equations for a multicomponent nonequilibrium gas are obtained from the more general equation of Ref. 7 and become the following:

Continuity

$$\frac{\partial}{\partial x}(\rho u r_b{}^j) + \frac{\partial}{\partial y}(\rho v r_b{}^j) = 0 \tag{1a}$$

Momentum

$$\rho u \frac{\partial u}{\partial x} + \rho v \frac{\partial u}{\partial y} = -\frac{dp_e}{dx} + \frac{\partial}{\partial y}\left(\mu \frac{\partial u}{\partial y}\right) \tag{1b}$$

Energy

$$\bar{c}_p \rho u \frac{\partial T}{\partial x} + \bar{c}_p \rho v \frac{\partial T}{\partial y} = u \frac{dp_e}{dx} + \mu \left(\frac{\partial u}{\partial y}\right)^2 + \frac{\partial}{\partial y}\left(k \frac{\partial T}{\partial y}\right) - \sum_{k=1}^{NI} c_{pi} j_i \frac{\partial T}{\partial y} - \sum_{i=1}^{NI} h_i w_i \tag{1c}$$

Species Continuity

$$\rho u \frac{\partial c_i}{\partial x} + \rho v \frac{\partial c_i}{\partial y} = -\frac{\partial}{\partial y}(j_i) + w_i \tag{1d}$$

Since,

$$\sum_{i=1}^{NI} c_i = 1 \tag{1e}$$

there are only (NI-1) independent species continuity equations (1d), and Eq. (1e) is used to determine c_{NI}. For two-dimensional flow, $j = 0$, and for axisymmetric flow, $j = 1$. The expression for the mass flux j_i in a multicomponent mixture of perfect gases for the boundary layer is given in Ref. 7 and is written in the following form:

$$j_i = \frac{\mu}{Pr}\left\{\sum_{k=1}^{NI} \bar{\bar{b}}_{ik} \frac{\partial c_k}{\partial y} - \frac{L_i{}^T}{T} \frac{\partial T}{\partial y}\right\} \tag{2}$$

where

$$\bar{\bar{b}}_{ik} = \frac{M_i}{\bar{M}}\left(L_{ik} - \frac{\bar{M}}{M_k} \sum_{j=1}^{NI} L_{ij} c_j\right)$$

The pressure diffusion term is neglected due to the boundary-layer assumption, and the forced diffusion term is assumed zero in the preceding expression for the mass flux. To complete the preceding equations, the equation of state

$$\rho = p_e \Big/ RT \sum_{i=1}^{NI} \frac{c_i}{M_i} \tag{3}$$

is required. This equation assumes the gas consists of a mixture of chemically-reacting perfect gases and assumes that the pressure change across the boundary layer is negligibly small.

The preceding boundary-layer equations are transformed with the Mangler and Howarth-Dorodnitsyn transformation in order to obtain them in a form more appropriate for numerical solution. The new independent variables introduced are

$$\xi(x) = \int_0^x (\rho\mu)_r u_e r_b{}^{2j} dx \tag{4a}$$

$$\eta(x, y) = \frac{u_e r_b{}^j}{(2\xi)^{1/2}} \int_0^y \rho dy \tag{4b}$$

and derivatives become

$$\frac{\partial}{\partial x} = (\rho\mu)_r u_e r_b{}^{2j} \frac{\partial}{\partial \xi} + \frac{\partial \eta}{\partial x} \frac{\partial}{\partial \eta} \tag{5a}$$

$$\frac{\partial}{\partial y} = \frac{\rho u_e r_b{}^j}{(2\xi)^{1/2}} \frac{\partial}{\partial \eta} \tag{5b}$$

When the new dependent variables

$$V = \frac{2\xi}{(\rho\mu)_r u_e r_b{}^{2j}}\left(f' \frac{\partial \eta}{\partial x} + \frac{\rho v r_b{}^j}{(2\xi)^{1/2}}\right) \tag{6a}$$

$$f' = u/u_e \tag{6b}$$

$$\theta = T/T_e \tag{6c}$$

$$c^* = c_i/c_{ir} \tag{6d}$$

are introduced, and the transformations (5) are applied, the boundary-layer equations become the following in the transformed plane:

Continuity

$$2\xi \frac{\partial f'}{\partial \xi} + \frac{\partial V}{\partial \eta} + f' = 0 \tag{7a}$$

Momentum

$$2\xi f' \frac{\partial f'}{\partial \xi} + V \frac{\partial f'}{\partial \eta} = \beta\left[\frac{\bar{M}_e}{\bar{M}} \theta - (f')^2\right] + \frac{\partial}{\partial \eta}\left(l \frac{\partial f'}{\partial \eta}\right) \tag{7b}$$

Energy

$$2\xi f' \frac{\partial \theta}{\partial \xi} + V \frac{\partial \theta}{\partial \eta} = \frac{u_e{}^2}{\bar{c}_p T_e}\left[l\left(\frac{\partial f'}{\partial \eta}\right)^2 - \beta \frac{\bar{M}_e}{\bar{M}} f'\theta\right] + \frac{1}{\bar{c}_p}\frac{\partial}{\partial \eta}\left(\frac{l\bar{c}_p}{Pr}\frac{\partial \theta}{\partial \eta}\right) - \sum_{i=1}^{NI} \frac{c_{pi}}{\bar{c}_p}\left(j_i \frac{r_b{}^j (2\xi)^{1/2}}{d\xi/dx}\right)\frac{\partial \theta}{\partial \eta} - \frac{2\xi}{\bar{c}_p T_e u_e d\xi/dx} \sum_{i=1}^{NI} h_i \left(\frac{w_i}{\rho}\right) - \frac{2\xi\theta f'}{T_e}\frac{dT_e}{d\xi} \tag{7c}$$

Species Continuity (i = 1, 2, ... NI-1)

$$2\xi f' \frac{\partial c_i{}^*}{\partial \xi} + V \frac{\partial c_i{}^*}{\partial \eta} = -\frac{\partial}{\partial \eta}\left(\frac{r_b{}^j (2\xi)^{1/2}}{d\xi/dx}\frac{j_i}{c_{ir}}\right) + \frac{2\xi}{c_{ir} u_e d\xi/dx}\left(\frac{w_i}{\rho}\right) \tag{7d}$$

$$c_{NI}{}^* = \frac{1}{c_{NIr}}\left[1 - \sum_{i=1}^{NI-1} c_i{}^* c_{ir}\right]$$

The mass flux in the transformed plane becomes

$$\frac{r_b{}^j (2\xi)^{1/2}}{d\xi/dx} j_i = \left\{\sum_{k=1}^{NI} (c_k r b_{ik}) \frac{\partial c_k{}^*}{\partial \eta} - \frac{l}{Pr}\frac{L_i{}^T}{\theta}\frac{\partial \theta}{\partial \eta}\right\} \tag{8}$$

where

$$b_{ik} = \frac{l}{Pr}\frac{M_i}{\bar{M}}\left(L_{ik} - \frac{\bar{M}}{M_k} \sum_{j=1}^{NI} c_{jr} L_{ij} c_j{}^*\right) = \frac{l}{Pr}\bar{\bar{b}}_{ik}$$

The system of equations (7) governs the multicomponent boundary-layer flow that will be solved numerically. The

conditions at the wall and the outer edge of the boundary layer determine the necessary boundary conditions for these equations. At the wall, it is assumed that the normal and tangential velocities are zero, the wall temperature is specified, and the mass fraction of the species is also specified. These conditions in the transformed coordinates become

$$f'(\xi, 0) = 0$$
$$V(\xi, 0) = 0$$
$$\theta(\xi, 0) = \theta_b(\xi)$$
$$c_i(\xi, 0) = c_{ib}(\xi) \qquad i = 1, 2, \ldots NI\text{-}1$$

These boundary conditions correspond to the assumption of a catalytic wall when equilibrium composition is used at the wall. The element mass fraction of oxygen or nitrogen is required to determine the equilibrium composition and is unknown when multicomponent diffusion is employed. If all of the binary Lewis-Semenov numbers are equal, the mass fraction of the elements are constant across the boundary layer. It has been assumed that the mass fraction of the elements at the wall are the same as those at the boundary-layer edge, and this is reasonable for the present examples as shown in Ref. 1. For different assumptions, e.g., specified heat-transfer and noncatalytic wall, the preceding boundary conditions are replaced by requiring certain gradients to be satisfied at the wall.

The flow at the outer edge of the boundary layer is determined from inviscid nonequilibrium flow along the body surface (see Sec. C). The boundary conditions at the outer edge are $f \to 1$, $\theta \to 1$, $c_i \to c_{ie}$.

It may be noticed that, although the temperature and velocity at the outer edge do not appear in these boundary conditions, these quantities appear as parameters in the partial differential equations.

B. Chemical Reactions and Production Term

For a multicomponent gas with NI distinct chemical species and NR simultaneous chemical reactions, the stoichiometric relations are

$$\sum_{i=1}^{NJ} \alpha_{ri} X_i \underset{k_{br}}{\overset{k_{fr}}{\rightleftarrows}} \sum_{i=1}^{NJ} \beta_{ri} X_i \qquad (r = 1, 2, \ldots NR) \tag{9}$$

The quantities X_i represent the chemical species, and α_{ri} and β_{ri} are the stoichiometric coefficients. Also, an X_i can represent a catalytic body that consists of a linear combination of the other species, and for this case NJ is equal to the number of species NI plus the number of these catalytic bodies. The net mass rate of production of species i per unit volume is the sum of the mass rate of production of species i per unit volume from each reaction and is usually written as

$$w_i = M_i \sum_{r=1}^{NR} (\beta_{ri} - \alpha_{ri}) \left[k_{f_r} \prod_{j=1}^{NJ} (\rho\gamma_j)^{\alpha_{rj}} - k_{b_r} \prod_{j=1}^{NJ} (\rho\gamma_j)^{\beta_{rj}} \right] \tag{10}$$

The mass concentration γ_j for the NI species is

$$\gamma_j = c_j/M_j \qquad j = 1, 2, \ldots NI \tag{11a}$$

whereas for the catalytic bodies, the following expression is used for the fictitious species:

$$\gamma_j = \sum_{i=1}^{NI} Z_{(j-NI)i}\, \gamma_i \qquad j = NI + 1, \ldots NJ \tag{11b}$$

The constants $Z_{(j-NI)i}$ are determined from the linear dependence of the catalytic bodies upon the NI species. The production term is evaluated by the method suggested by Emanuel and Vincenti.[8]

C. Initial Profiles and Exterior Flow

In order to start the solution of the parabolic type partial differential equations, initial profiles of the dependent variables (V, f', θ, c_i, c_2 ... c_{NI-1}) are required. At the start of the boundary layer, $\xi = 0$, and the partial differential equations (7) become ordinary differential equations. Thus, the initial conditions for the finite-difference method are those exactly for $\xi = 0$. These equations have been considered by Blottner and Lenard,[1] and the required initial profiles were obtained from the resulting computer program.

To obtain the inviscid flow along the surface of the body or at the edge of the boundary layer, the ordinary differential equations for a streamtube are solved. Also at the same time, the relation between the transformed coordinate ξ and the distance x along the surface can be determined from Eq. (4a).

In order to solve the equations, it is necessary to know the pressure gradient along the body which should be obtained from the inviscid nonequilibrium flow field solution, but a reasonable estimate can be obtained from the equilibrium flow field. The solutions of the ordinary differential equations are obtained with the Runge-Kutta method, with the procedure for changing the step-size as developed by Emanuel[9] for nonequilibrium nozzle flows. When the desired flow field is known, the quantities u_e, T_e, p_e, c_{i_e}* along the body can be imputed to the program.

D. Method of Solution

The partial differential equations (7) are solved with a Crank-Nicolson[10] type of implicit finite-difference scheme which has been developed for the boundary-layer equations for nonequilibrium flow of a binary gas by Blottner.[6] The details of replacing the derivatives by difference quotients such that one obtains the difference equations

$$A_n w_{n+1} + B_n w_n + C_n w_{n-1} = D_n \tag{12}$$

are given in Ref. 11. The continuity equation (7a) is not used in the preceding difference equations, but is required after these equations are solved. Since the simultaneous linear algebraic equations resulting from all of the difference equations (12) across the boundary layer are of a special form, an efficient method of solution on a digital computer is available[12] and is applied to the equations for the boundary layer in Ref. 11. For this procedure, the boundary conditions at the wall and outer edge are written in matrix notation as

$$w_1 = Hw_2 + Fw_3 + h \tag{13a}$$
$$w_N = g \tag{13b}$$

Then with boundary conditions (13) and expressions (12), the dependent variables are computed across the boundary layer. This procedure gives all of the desired quantities except V at a small distance $\Delta\xi$ downstream from the known boundary-layer profiles. The continuity equation (7a) is used to obtain V and is written in the following finite difference form:

$$V_{m+1/2,n} = V_{m+1/2,n-1} - \Delta\eta \left(\frac{\xi}{\Delta\xi} + \frac{1}{4} \right) (f'_{m+1,n} + f'_{m+1,n-1}) + \Delta\eta \left(\frac{\xi}{\Delta\xi} - \frac{1}{4} \right) (f'_{m,n} + f'_{m,n-1}) \tag{14}$$

The foremention procedure is applied at succeeding steps downstream until the boundary-layer flow along the body is determined.

III. Numerical Calculations

A. Gas Model

The multicomponent gas model is now applied to ionized air with the following chemical species: N, O, O_2, N_2, NO, NO^+. The electrons are not considered separately, as they are assumed to diffuse with the ions as considered by Blottner and Lenard.[1]

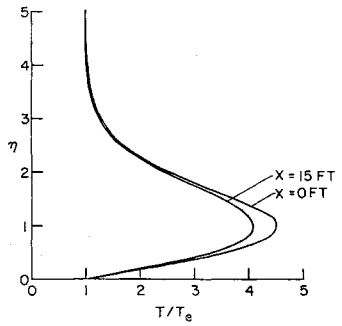

Fig. 1 Temperature profiles for the boundary layer on a 10° cone at 100,000 ft.

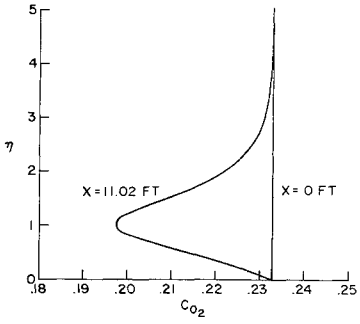

Fig. 3 Mass fraction of molecular oxygen across the boundary layer on a 10° cone at 100,000 ft.

The chemical reactions below are considered for the ionized boundary-layer flow:

$$r = 1: \quad O_2 + O_2 \rightleftarrows 2O + O_2 \tag{15}$$

$$= 2: \quad O_2 + O \rightleftarrows 2O + O \tag{16}$$

$$= 3: \quad O_2 + M^{(1)} \rightleftarrows 2O + M^{(1)}, \quad M^{(1)} = N, N_2, NO \tag{17}$$

$$= 4: \quad N_2 + N_2 \rightleftarrows 2N + N_2 \tag{18}$$

$$= 5: \quad N_2 + N \rightleftarrows 2N + N \tag{19}$$

$$= 6: \quad N_2 + M^{(2)} \rightleftarrows 2N + M^{(2)}, \quad M^{(2)} = O, O_2, NO \tag{20}$$

$$= 7: \quad NO + M^{(3)} \rightleftarrows N + O + M^{(3)}, \quad M^{(3)} = O, O_2, N, N_2 \tag{21}$$

$$= 8: \quad NO + O \rightleftarrows O_2 + N \tag{22}$$

$$9: \quad N_2 + O \rightleftarrows NO + N \tag{23}$$

$$= 10: \quad N_2 + O_2 \rightleftarrows 2NO \tag{24}$$

$$= 11: \quad N + O \rightleftarrows NO^+ + e^- \tag{25}$$

The reaction rate constants employed for the preceding chemical reactions are those given by Bortner.[13]

The thermodynamic properties of the species (enthalpy and specific heat) have been obtained from tabulated values[20] computed by the usual statistical mechanics procedures. The atomic species properties include translation and electronic excitation energy and are in excellent agreement with Gilmore's[14] results below 15,000°K. The diatomic species use the rigid rotator-harmonic oscillator model with corrections for rotational stretching and vibrational anharmonicity following the work of Mayer and Mayer.[15] The properties of the diatomic species are similar to the results of Beckett and Haar[16] with the exception of NO^+ above 6000°K, whereas the results differ somewhat from Gilmore[14] at the higher temperatures. The results of Beckett and Haar appear to be incorrect for NO^+.

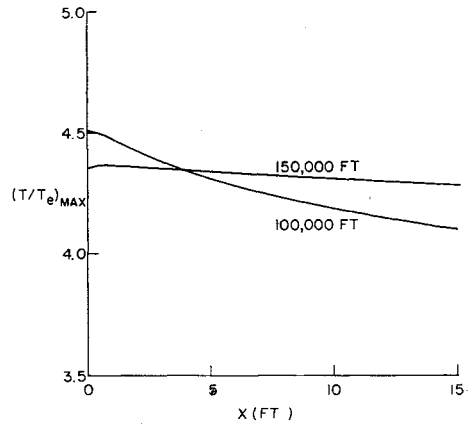

Fig. 2 Maximum temperature in the boundary layer on a 10° cone.

The viscosity and thermal conductivity are calculated by means of Wilke's semiempirical formula (see Ref. 7, pp. 24 and 257). The viscosity of the species was obtained with the collision integrals for dissociated air given by Yun and Mason.[17] The viscosity of NO^+ was assumed the same as that of NO. The collision integrals of Ref. 17 were also used to evaluate the neutral binary diffusion coefficients with interactions N-O_2 and N-NO assumed the same as N-N_2. The binary diffusion coefficients for the NO^+ ions were obtained from Baulknight,[18] based on a charged-induced dipole for the potential energy. For more details of the thermodynamic transport properties, the reader is referred to Ref. 11. The thermal diffusion is neglected in the following examples.

For the ambipolar diffusion of the ions and electrons, it has been shown by Blottner and Lenard that the binary diffusion coefficient $\mathfrak{D}_{NO^+j}$ must be doubled in the calculations for the multicomponent diffusion coefficients. In addition, the mass flux for NO^+ is treated as a trace species, as this eliminates numerical round-off errors that occur otherwise. Even with this approximation, the mass flux for NO^+ is accurately given as

$$j_{NO^+} = -\frac{2\mu}{Pr} Le_{NO^+} \frac{\partial c_{NO^+}}{\partial y}$$

where

$$Le_{NO^+} = \sum_{\substack{j=1 \\ j \neq NO^+}}^{NI} \frac{c_j}{M_j} \Bigg/ \sum_{\substack{j=1 \\ j \neq NO^+}}^{NI} \frac{c_j}{M_j \mathfrak{L}_{NO^+ j}}$$

B. Specific Examples

The flow along a sharp cone with 10° half angle has been computed with the infinite-difference scheme for the ionized air. The pressure along the cone has been taken as a constant, and the edge of the boundary layer is used as the reference for the density-viscosity product. The cone is considered at a velocity of 22,000 fps and two altitudes that results in the following conditions at the outer edge of the boundary layer (Table 1). At the wall, the temperature was specified as 1000°K, whereas the mass fraction of the various species were taken equal to the equilibrium composition based on the wall temperature and element mass fraction at the tip. The initial profiles at the tip of the cone were obtained from Blottner and Lenard,[3] and then the finite-difference method was employed to obtain the solution as far as 15-ft downstream.

The variation of temperature across the boundary layer at 100,000 ft is given in Fig. 1. The maximum temperature

Table 1

h = 100,000 ft	h = 150,000 ft
u_e = 21,590 fps	u_e = 21,590 fps
T_e = 1019 °K	T_e = 1061 °K
P_e = 522.6 psf	P_e = 58.323 psf

in the boundary layer at the two altitudes considered is shown in Fig. 2. At 150,000 ft, there is approximately a 50°K drop in maximum temperature, whereas at 100,000 ft, the decrease has become 400°K. In both cases, the temperature is not near the temperature corresponding to chemical equilibrium.

Near the tip of the cone, the gas is undissociated, and because of the high temperature peak in the boundary layer, the gas begins to dissociate downstream. Figures 3 and 4 illustrate this as the molecular oxygen and nitrogen decreases

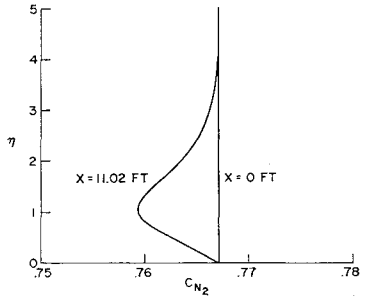

Fig. 4 Mass fraction of molecular nitrogen across the boundary layer on a 10° cone at 100,000 ft.

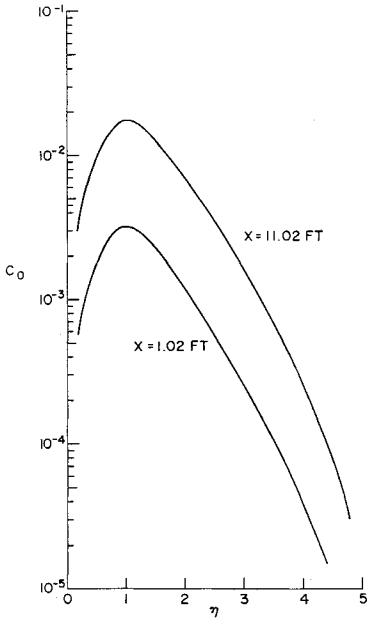

Fig. 5 Mass fraction of atomic oxygen across the boundary layer on a 10° cone at 100,000 ft.

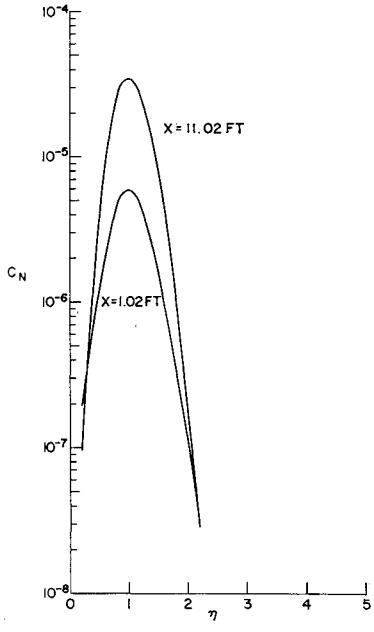

Fig. 6 Mass fraction of atomic nitrogen across the boundary layer on a 10° cone at 100,000 ft.

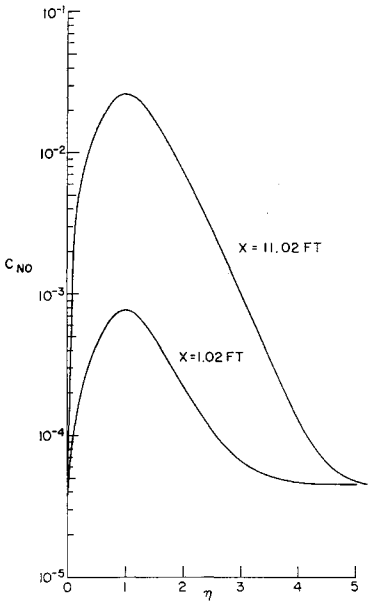

Fig. 7 Mass fraction of nitric oxide across the boundary layer on a 10° cone at 100,000 ft.

in the flow downstream. At 15 and 100,000 ft, about 16% of the oxygen is dissociated and 2% of the nitrogen is dissociated. The variation of atomic oxygen, atomic nitrogen, nitric oxide, and electron density across the boundary layer is given in Figures 5–8, respectively. The electron density is obtained from the mass fraction of NO^+ with the relation

$$N_e = \bar{\rho}\,(\bar{N}/M_{NO^+})c_{NO^+}$$

where

$$\bar{N} = 6.025 \times 10^{23} \text{ molecules/g-mole}$$

$$\bar{\rho} = 0.51536\,\rho \text{ g/cm}^3$$

The atomic nitrogen profiles tend to be thinner, whereas the electron density gives a thicker boundary layer.

It is important to notice that the oxygen atom profiles are of similar shape along the cone. Therefore, we can express this as

$$c_O = c_{O\max}(\xi)P(\eta)$$

where $P(\eta_{\max}) = 1$ and $(\partial P/\partial\eta)_{\max} = 0$. When the foregoing

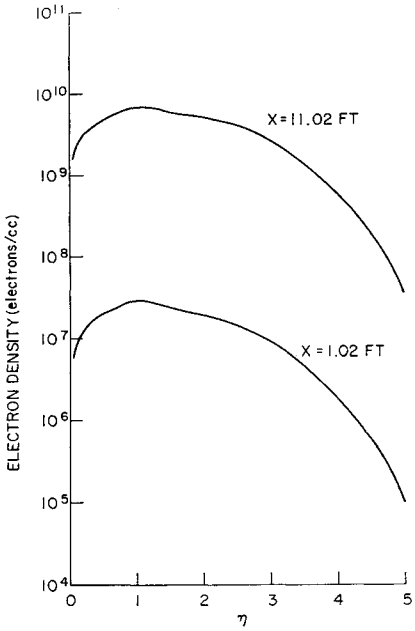

Fig. 8 Electron density in the boundary layer on 10° cone at 100,000 ft.

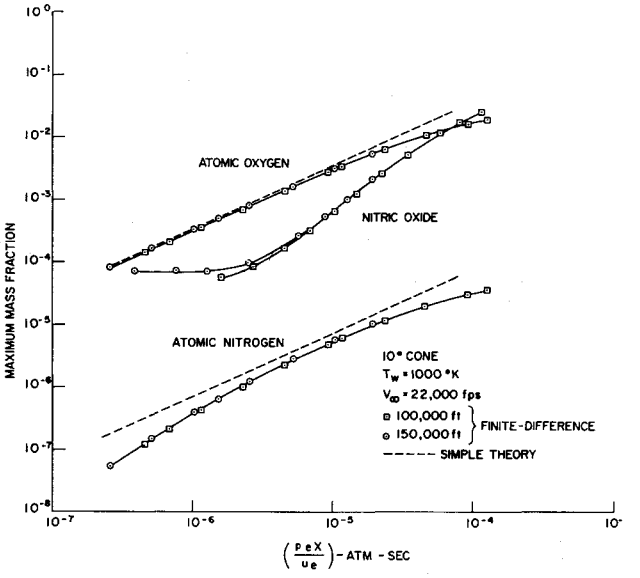

Fig. 9 Peak atomic oxygen, atomic nitrogen, and nitric oxide.

is substituted into Eq. (7d) with the assumptions of "local similarity," Fick's law for diffusion, and constant density-viscosity product and Schmidt number, Sc_O; the following is obtained:

$$c_{O\max} = -\frac{2Sc_O}{3lP''(\eta_{\max})}\left(\frac{\rho_e x}{u_e}\right)\left(\frac{w_O}{\rho_e \rho}\right)$$

This equation has been evaluated with $P''(\eta_{\max})$ determined from the profiles, $Sc_O = 0.5$, $l = 1$, and the production term $(w_O/\rho_e\rho)$ obtained from Eq. (1) of Ref. 4. The result of this computation is shown in Fig. 9 along with the finite-difference results. The variation of atomic nitrogen was determined with Eq. (3) of Ref. 4 with the present mass fraction of atomic oxygen in the expression. This result and the finite-difference data are given in Fig. 9. The preceding relation is useful because it shows how one can correlate the results near the tip of the cone. The maximum amount of nitric oxide is also presented in Fig. 9 for the finite-difference results.

The NO^+ profiles are of similar shape along the cone, and expressions corresponding to the ones for oxygen can be obtained. In terms of the electron density, the following is obtained:

$$\frac{N_e}{\rho_e} \sim \frac{Sc_{NO^+}Sc_O{}^2}{l^3}\frac{e^{-185{,}000/T_p}}{T_p{}^{6.5}}\left(\frac{\rho_e x}{u_e}\right)^3 \tag{26}$$

where T_p is the peak temperature (°K) in the boundary layer at the tip of the cone. The maximum electron density is given in Fig. 10 and has been correlated as indicated by the foregoing expression. Additional finite-difference results have been included in order to show the validity of this correlation. If the local peak temperature is employed rather than T_p, the correlation could perhaps be extended further downstream. The multistrip results of Pallone, Moore, and Erdos[2] and the approximate theory of Levinsky and Fernandez[4] are also shown in this figure. It should be noted that this type of correlation is valid only for low wall temperatures.

The effect of the thermodynamic properties of the air system on the peak electron density has been investigated by including only the translation, rotation, and vibration energies in computing the enthalpy and specific heat. For these simpler thermodynamic properties, the peak electron density is slightly higher as shown in Fig. 11. When the rate constants of Wray[19] rather than those of Bortner[13] are employed, the electron density is increased as illustrated in Fig. 11. Rather than use the multicomponent diffusion, Fick's law has been employed with the binary Lewis-Semenov numbers constant and equal to 1.4. The electron density was only slightly changed with the simpler diffusion velocity. The influence of the transport properties on the electron density can be seen in Eq. (26). There are the explicit effects of the Schmidt numbers of NO^+ and O, and the density-viscosity product. Since the transport properties change the temperature T_p in the boundary layer, there is this additional influence on the electron density.

The production of the various species near the maximum temperature has been investigated. The production of atomic oxygen comes almost entirely from the three oxygen dissociation reactions (15–17). The three reactions can have nearly equal importance in producing atomic oxygen. The nitric oxide dissociation reaction (21) produces a very small amount of atomic oxygen. The shuffle reaction (22) produces atomic oxygen, whereas shuffle reaction (23) consumes atomic oxygen which results in a slight consumption of atomic oxygen for the two reactions. The production of nitric oxide in the flow near $\eta = 1$ is shown

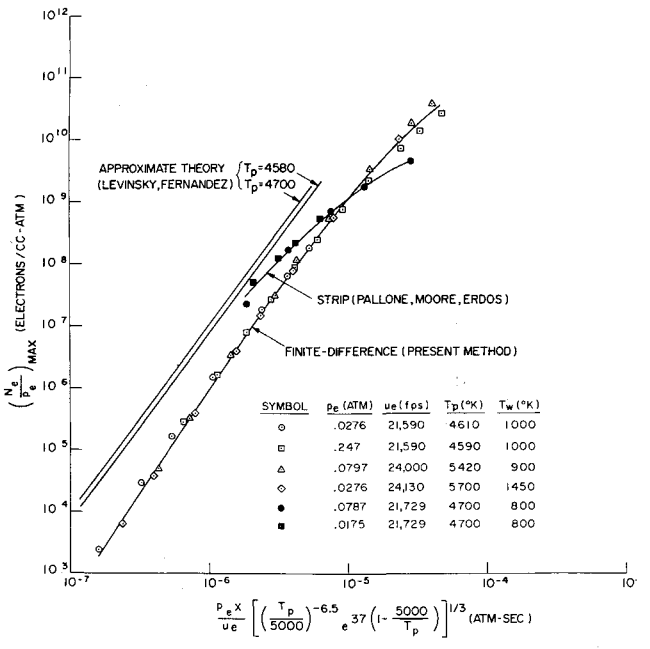

Fig. 10 Maximum electron density in the boundary layer.

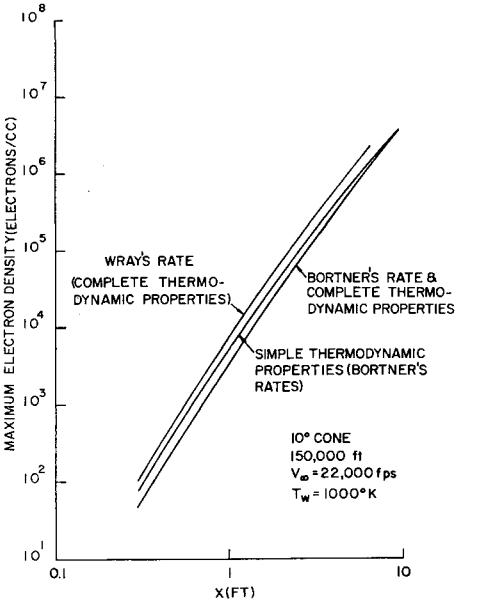

Fig. 11 Effect of thermodynamic properties and rate constants on electron density.

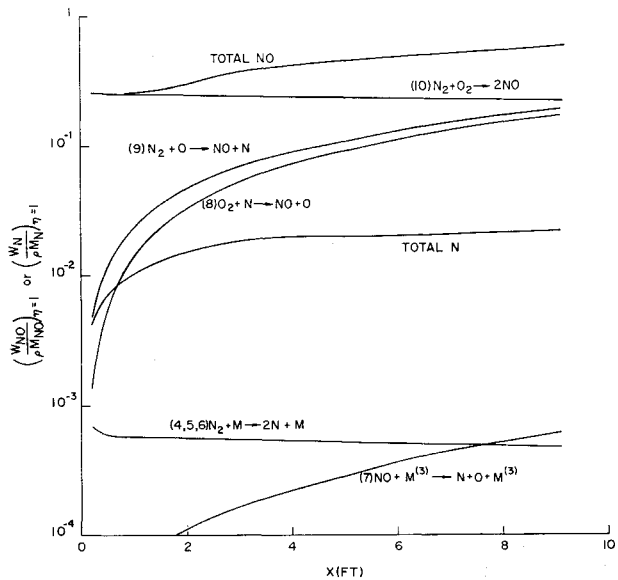

Fig. 12 Production of nitric oxide and nitrogen in the boundary layer at 150,000 ft.

in Fig. 12. The shuffle reactions (22–24) are producing nitric oxide, and the dissociation reaction (21) is reducing nitric oxide by a negligible amount. The production of atomic nitrogen from the various reactions is also given in Fig. 12. The direct dissociation of nitrogen by reactions (18–20) produces a small amount of atomic nitrogen. Near the tip the shuffle reactions are the dominant reactions for producing atomic nitrogen. Shuffle reaction (23) is producing atomic nitrogen at a faster rate than shuffle reaction (22) is consuming the element. Downstream, the nitric oxide dissociation reaction (21) becomes more important in producing atomic nitrogen. The production of electrons results from reaction (25) and, because of this reaction, a negligible amount of atomic oxygen and nitrogen is consumed.

Computations of the boundary layer have been made with shuffle reaction (24) omitted, and the electron density was only slightly changed. This reaction is the main producer of NO near the tip of the cone where reaction (21) is not very important in producing N. When reaction (21) becomes important in producing N, the shuffle reaction (24) is no longer the dominant producer of NO. Therefore, the shuffle reaction (24) has a small effect on the total amount of atomic nitrogen, and hence electron density, in the boundary layer flow on cones.

References

[1] Blottner, F. G. and Lenard, M., "Finite rate plasma generation in the laminar air boundary layer of slender reentry bodies," *Transactions of the Eighth Symposium on Ballistic Missile and Space Technology* (Air Force Space Systems Printing Division, Los Angeles, Calif., 1963), pp. 3–33.

[2] Pallone, A., Moore, J., and Erdos, J., "Nonequilibrium, nonsimilar solutions of the laminar boundary layer equations," Avco RAD-TM-63-58 (November 19, 1963).

[3] Lenard, M., "Chemically reacting boundary layers," General Electric Missile and Space Div., Space Sciences Lab. TIS Rept. R64SD14 (March 1964).

[4] Levinsky, E. S. and Fernandez, F. L., "Approximate nonequilibrium air ionization in hypersonic flows over sharp cones," AIAA J. **2**, 565–568 (1964); also Aerospace Corp. TDR 269 (54810-60)-1 (November 7, 1964).

[5] DeRienzo, R., Wood, A. D., Berner, F., and Teare, J. D., "Effects of nonequilibrium on the hypersonic laminar air boundary layer," *Transactions of the Eighth Symposium on Ballistic Missile and Space Technology* (Air Force Space Systems Printing Division, Los Angeles, Calif., 1963), Vol. II, pp. 35–64.

[6] Blottner, F. G., "Chemical nonequilibrium boundary layer," AIAA J. **2**, 232–240 (1964).

[7] Bird, R. B., Stewart, W. E., and Lightfoot, E. N., *Transport Phenomena* (John Wiley & Sons, Inc., New York, 1960), Chap. 18.

[8] Emanuel, G. and Vincenti, W. G., "Method of calculation of the one-dimensional non-equilibrium flow of a general gas mixture through a hypersonic nozzle," Arnold Engineering Development Center AEDC-TDR-62-131 (June 1962).

[9] Emanuel, G., "Problems underlying the numerical integration of the chemical and vibrational rate equations in a near-equilibrium flow," Arnold Engineering Development Center AEDC-TDR-63-82 (March 1963).

[10] Crank, J. and Nicolson, P., "A practical method for numerical evaluation of solutions of partial differential equations of the heat conduction type," Proc. Cambridge Phil. Soc. **42**, 50(1947)

[11] Blottner, F. G., "Non-equilibrium laminar boundary layer flow of ionized air," General Electric TIS Rept. R64SD56.

[12] Richtmyer, R. D., *Difference Methods for Initial-Value Problems* (Interscience Publishers, Inc., New York, 1957), Chap. 9.

[13] Bortner, M. H., "Chemical kinetics in a re-entry flow field," General Electric TIS R63SD63 (August 1963).

[14] Gilmore, F. R., "Equilibrium composition and thermodynamic properties of air to 25,000°K," Rand Corp. Rept. RM-1543 (August 24, 1955).

[15] Mayer, J. E. and Mayer, M. G., *Statistical Mechanics* (John Wiley & Sons, Inc., New York, 1940).

[16] Beckett, G. W. and Haar, L., "Thermodynamic properties at high temperatures: ideal gas thermal functions to 25,000°K for diatomic molecules, oxygen, nitrogen, nitric oxide, and their molecule ions," *Proceedings of the Joint Conference on Thermodynamic and Transport Properties of Fluids* (Institute of Mechanical Engineers, London, 1958).

[17] Yun, K. S. and Mason, E. A., "Collision integrals for the transport properties of dissociating air at high temperatures," Phys. Fluids **5**, 380–386 (1962).

[18] Baulknight, C. W., "Binary diffusion coefficients for NO^+," General Electric Missile and Space Div. internal communication (unpublished).

[19] Wray, K. L., "Chemical kinetics of high temperature air," *ARS Progress in Astronautics and Rocketry: Hypersonic Flow Research*, edited by F. R. Riddell (Academic Press Inc., New York, 1962), Vol. 7, pp. 181–204.

[20] Browne, W. G., private communication (May 1962).